A New Population of Parvocellular Oxytocin Neurons Controlling Magnocellular Neuron Activity and Inflammatory Pain Processing

Marina Eliava, Meggane Melchior, H. sophie Knobloch-Bollmann, Jérôme Wahis, Miriam Da Silva Gouveia, Yan Tang, Alexandru Cristian Ciobanu, Rodrigo Triana Del Rio, Lena C. Roth, Ferdinand Althammer, et al.

A new population of parvocellular oxytocin neurons controlling magnocellular neuron activity and inflammatory pain processing

Running title: Oxytocin Neuron Cross-Talk Attenuates Nociception

Marina Eliava[1@], Meggane Melchior[2@], H. Sophie Knobloch-Bollmann[1,3%@], Jérôme Wahis[2@], Miriam da Silva Gouveia[1], Yan Tang[1,5], Alexandru Cristian Ciobanu[4], Rodrigo Triana del Rio[4], Lena C. Roth[1,3], Ferdinand Althammer[1], Virginie Chavant[2], Yannick Goumon[2], Tim Gruber[1,3], Nathalie Petit-Demoulière[2], Marta Busnelli[6], Bice Chini[6,7], Linette L. Tan[8], Mariela Mitre[9], Robert C. Froemke[9], Moses V. Chao[9], Günter Giese[3], Rolf Sprengel[3], Rohini Kuner[8], Pierrick Poisbeau[2], Peter H. Seeburg[3], Ron Stoop[4*], Alexandre Charlet[2,10*#], and Valery Grinevich [1,3,11*#]

[1]Schaller Research Group on Neuropeptides at German Cancer Research Center (DKFZ) and CellNetwork Cluster of Excellence at the University of Heidelberg, Heidelberg, Germany;
[2]Centre National de la Recherche Scientifique, Institut National de la Santé et de la Recherche Médicale and University of Strasbourg, Institute of Cellular and Integrative Neurosciences, 5 rue Blaise Pascal, 67084, Strasbourg, France;
[3]Max Planck Institute for Medical Research, Heidelberg, Germany;
[4]Center for Psychiatric Neurosciences, Hôpital de Cery, Lausanne University Hospital (CHUV), Lausanne, Switzerland;
[5]East China Normal University, Shanghai, China;
[6]National Research Council, Institute of Neuroscience, Milan, Italy.
[7]Humanitas Clinical and Research Center, via Manzoni 56, 20089, Rozzano, Italy
[8]Department for Molecular Pharmacology and Molecular Medicine Partnership Unit with European Molecular Biology Laboratories, Institute of Pharmacology, Heidelberg University, Heidelberg, Germany;
[9]New York University School of Medicine, Skirball Institute of Biomolecular Medicine, New York, USA;
[10]University of Strasbourg Institute for Advanced Study (USIAS), Strasbourg, France.
[11]Central Institute of Mental Health (ZI), Mannheim, Germany
[%]Present address: Department of Molecular and Cellular Biology, Center for Brain Science, Harvard University, 52 Oxford Street, Cambridge, MA 02139, USA

[@] Co-first author
* Co-senior author
[#] Corresponding author

Corresponding authors:

Alexandre Charlet, PhD
CNRS
University of Strasbourg
INCI, UPR2112
USIAS Fellow, Group on Molecular Determinants of Pain
5, rue Blaise Pascal
67084 Strasbourg, France
Phone: + 33 (0) 6070 825 06
E-mail: acharlet@unistra.fr

Valery Grinevich, MD, PhD
Schaller Research Group on Neuropeptides (V078)
German Cancer Research Center (DKFZ)
Central Institute of Mental Health (ZI)
CellNetwork Cluster of Excellence
University of Heidelberg
Im Neuenheimer Feld 581
D-69120 Heidelberg, Germany
Phone: + 49 (0) 6221 42 1581
E-mail: v.grinevich@Dkfz-Heidelberg.de

SUMMARY

Oxytocin (OT) is a neuropeptide elaborated by the hypothalamic paraventricular (PVN) and supraoptic (SON) nuclei. Magnocellular OT neurons of these nuclei innervate numerous forebrain regions and release OT into the blood from the posterior pituitary. The PVN also harbors parvocellular OT cells that project to the brainstem and spinal cord, but their function has not been directly assessed. Here, we identified a subset of approximately 30 parvocellular OT neurons, with collateral projections onto magnocellular OT neurons and neurons of deep layers of the spinal cord. Evoked OT release from these OT neurons suppresses nociception and promotes analgesia in an animal model of inflammatory pain. Our findings identify a new population of OT neurons that modulates nociception in a two tier process: 1) directly by release of OT from axons onto sensory spinal cord neurons and inhibiting their activity, 2) indirectly by stimulating OT release from SON neurons into the periphery.

INTRODUCTION

Oxytocin (OT), a neuropeptide that plays an important role in sociability, is produced in the brain exclusively in the hypothalamic paraventricular (PVN), supraoptic (SON) and intermediate accessory nuclei (Swanson and Sawchenko, 1983). OT neurons can be classified in magnocellular OT (magnOT) and parvocellular OT (parvOT) neurons, which are distinct in size and shape, subnuclear location, the amount of OT production, and involvement in distinct circuitries and functions (Armstrong et al., 1980; Swanson and Kuypers, 1980; Sofroniew, 1983; Swanson and Sawchenko, 1983).

According to a long-held dogma, magnOT neurons provide systemic OT supply by release into the blood via the posterior pituitary (Scharrer, 1928; Scharrer and Scharrer, 1940, Bargmann and Scharrer, 1951). Simultaneously, magnOT neurons innervate the forebrain, including the nucleus accumbens (Ross et al., 2009; Knobloch et al., 2012; Dölen et al., 2013) and the central nucleus of the amygdala (Knobloch et al., 2012). The forebrain fibers, as exemplarily studied in the central amygdala, allow for focal release and discrete, modulatory action of OT (Knobloch et al., 2012). These characteristics might account for the distinct impact of OT on numerous types of brain-region specific behaviors (Lee et al., 2010).

In contrast to magnOT neurons, parvOT neurons project to distinct brainstem nuclei and different regions of the spinal cord (SC) (Swanson and Sawchenko, 1980; Sawchenko and Swanson, 1982). Based on the location of parvOT axons

and the effects of externally applied OT, it has been proposed that OT from parvOT axonal terminals contributes to modulation of cardiovascular functions, breathing, feeding behavior and nociception (Mack et al., 2002; Petersson, 2002; Condes-Lara et al., 2003; Atasoy et al., 2012). However, no selective and specific genetic access to parvOT neurons has been available and, hence, there was no evidence for the capacity of parvOT axons to release endogenous OT and to selectively modulate the above-mentioned functions. Moreover, it has remained unknown how parvOT neurons are incorporated into the entire OT system and functionally interact with magnOT neurons.

Based on recent reports that OT-modulated nociception and pain response comprise a peripheral (Juif and Poisbeau, 2013) and a central component (Juif et al., 2013; González-Hernández et al., 2014), it is tempting to propose that these components are dependent on different OT cell types. The central component results from parvOT innervation of SC targets (Swanson and McKellar, 1979), whereas peripherally acting OT, in contrast, is provided to the blood stream by magnOT neurons and presumably targets C-type fibers in the dorsal root ganglion (DRG; Juif and Poisbeau, 2013). We therefore hypothesized that the complementary, analgesic OT action – at central and peripheral levels – depends on the communication between magnOT and parvOT neurons residing in spatially segregated OT nuclei. Our present results reveal that the modulation of pain signals by OT is triggered by only a handful of parvOT neurons that innervate simultaneously “sensory wide dynamic range” (WDR) neurons in the deep laminae of the SC, expressing neurokinin-1 (NK1R) and OT receptors (OTR), and SON neurons that secrete OT in the periphery. We show that these

separate innervations underlie a two-tier modulation of pain by OT reaching the SC through fast, direct neuronal projections and a slower, indirect peripheral pathway.

RESULTS

Intrahypothalamic Axonal Trees of the OT System

To examine the intrahypothalamic OT system we used recombinant adeno-associated virus (rAAV) allowing cell-type specific fluorescent labeling of OT neurons with 98-100 % cell-type specificity, as reported in Knobloch et al., 2012. To compare the OT system with the vasopressin (VP) system we used AAV carrying different fluorescent markers driven by an evolutionarily conserved VP promoter (for specificity, see Table S1 and Figure S1A).

After injection of rAAV expressing Venus under the control of OT promoter (Figure 1A) we observed that OT neurons of the PVN give rise to fibers connecting to the ipsi- and even contralateral SON and form a pronounced plexus (Figure 1A4-A5). Interconnections within the intrahypothalamic VP system, in contrast, were absent (Figure S1C). The OT plexus might stem from PVN OT neurons projecting above the third ventricle to the contralateral PVN (Figure 1A3). OT connectivity from the PVN to SON was present in females and males (Figure S2A). The connection between the OT nuclei was one-way: SON-arising OT fibers reached only marginally the ipsi- (Figure 1A9), and never the contralateral SON (Figure 1A7) or PVN (Figure 1A8).

The OT PVN-SON connection was reconstructed using light sheet microscopy. As presented in Figure S2B, descending fibers from the PVN mainly project rostro-ventrally, turn horizontally at the level of the SON and enter the SON from

the rostral position, to run caudally along the whole extent of the nucleus.

PVN OT Neurons Innervate the SON and Control MagnOT Neuron Activity to Induce OT Release into Blood Circulation.

At the light microscopic level, Venus-labeled OT axons that arose from the PVN formed tight appositions to dendrites and somata of magnOT SON neurons resembling synaptic contacts. To assess if synapses were present, we injected the PVN with rAAV that expresses the synaptic marker synaptophysin fused to the green fluorescent marker EGFP in PVN OT neurons (Figure 1B1). GFP-positive puncta were found in the SON. The vast majority of terminals with GFP signal overlapped with VGluT2 signal (red, Figure 1B2). GFP/VGluT2 terminals engulfed OT cell bodies and dendrites (blue, Figure 1B2). We found that EGFP signals overlapped with VGluT2 in 92.6 ± 8.3 % of all terminals (Figure 1B2). These light microscopic observations suggested the presence of synaptic contacts, which we further confirmed at the electron microscopic level: EGFP-positive OT axons from the PVN (EGFP: greyish filling) formed asymmetric (presumably glutamatergic) synapses on OT dendrites of the SON (OT: dark aggregate in pre- and postsynaptic elements; Figure 1C1-C2).

Based on the anatomical evidence for OT connections between PVN and SON neurons, we aimed for a functional characterization of these connections. We expressed the blue-light (BL)-sensitive ChR2 protein (Nagel et al., 2003) fused to mCherry in PVN OT neurons (for construct validation see Knobloch et al., 2012). *In vivo* extracellular recordings in anaesthetized animals revealed the expression

of functional ChR2 in the PVN, as evident from BL-induced (PVN-BL, 20 s at 30 Hz with 10 ms pulses), reversible and reproducible increases of spike frequencies in these PVN neurons (on average the frequency increased from 4.1 ± 0.7 to 7.8 ± 0.7 Hz; data not shown).

We then further tested *in vivo* whether exposure to BL of PVN-OT axons in the SON (SON-BL, scheme in Figure 1D) could also activate, ipsilaterally, SON neurons. SON-BL exposure evoked a reversible increase in spike frequencies of SON neurons, from 6.7 ± 1.5 to 14.1 ± 2.7 Hz, confirming that BL stimulation of parvOT PVN axon terminals could excite SON neurons (Figure 1D1). To verify that OT was the main transmitter involved, we recorded the response of a single neuron to the SON-BL in the absence of any drug, or after sequential infusion of AMPA and OTR antagonists (respectively NBQX and dOVT) into the SON, and after their washout (Figure 1D2-D3). Interestingly, while NBQX decreased the baseline frequency of SON neurons, SON-BL paired to NBQX application still efficiently increased the relative frequency of discharge of the recorded neuron. Subsequent dOVT infusion totally blocked the SON-BL response, with full recovery 30 min after washout (Figure 1D2-D3). These results are in accordance with our previous observations in the central amygdala (Knobloch et al., 2012).

We aimed at providing functional evidence for the OT nature of the SON neurons that were contacted by the PVN. To this purpose we first of all injected into the blood circulation cholecystokinin (CCK), a hormone inducing the activation of OT neurons (Verbalis et al., 1986). CCK induced a prominent increase in spike frequencies of SON-BL responding neurons from 3.6 ± 0.8 to 15.0 ± 5.9 Hz

(Figure 1D1), establishing an indirect argument of the OT identity of the *in vivo* recorded SON neuron. Second, as magnOT neurons are known to release OT in the blood, we performed a time-dependent measurement of OT concentrations in plasma by mass-spectrometry after SON-BL. This revealed a significant increase of OT plasma concentrations at 60 s after SON-BL (from 0.84 ± 0.17 to 1.76 ± 0.22 pmol/ml, Figure 1E). Taken together, these findings provide evidence for an OT identity of the SON neurons that are activated by axonal terminals originating from OT neurons in the PVN.

OT Neurons Projecting to SON MagnOT Neurons Are ParvOT Neurons Displaying Distinct Anatomical and Electrophysiological Characteristics

To identify PVN neurons projecting to the SON we injected into the SON retrogradely transported and monosynaptically transmitted Canine adenovirus 2 (CAV2). After counting of sections containing the entire PVN, we identified in total a very small population of GFP/OT-positive neurons residing bilaterally (Table S2, 31.5 ± 8.5 neurons). CAV spread occurs within 200 μm of injection site (Schwarz et al., 2015), making unlikely the diffusion of the virus from the SON to PVN (the distance between these two nuclei is about 1.5 mm; see Paxinos and Watson, 1998).

To characterize the magno- *vs* parvocellular nature of back-labeled PVN cells we combined CAV2 with systemic administration of Fluorogold (Figure S3A). Fluorogold, when injected i.p., is taken up by neurons projecting beyond the blood brain barrier, *i.e.* by magnOT neurons thus allowing to distinguish them

from the parvOT (Fluorogold-negative) neurons (Lüther et al., 2002; Table S2). Notably, all magnOT neurons of the SON were Fluorogold-positive (not shown). After neuron counting in sections containing the entire PVN, we established that the vast majority of the 31.5 ± 8.5 GFP/OT-positive neurons (90 %) did not contain Fluorogold (Table S2). In addition to the detection of back-labeled GFP-positive neurons in the PVN, we observed GFP neurons in other structures typically known to innervate the SON, further confirming the specificity of our retrograde labeling (Miselis, 1981; Cunningham and Sawchenko, 1988; Figure S3B).

To characterize the parvOT neurons projecting to the SON, we next injected into the SON CAV2 expressing Cre recombinase and into the PVN rAAV carrying a double-floxed inverted ORF (DIO) of GFP under the control of the OT promoter (Figure 2A1). By this combination we limited GFP expression exclusively to SON-projecting parvOT neurons. In line with previous results, this revealed a unique position of back-labeled GFP neurons in the dorso-caudal PVN (Figure 2A2-A3, S2B-C). Individual GFP neurons have bipolar spindle-like morphology (Figure 2A4) distinct from neighboring magnOT neurons (Figure 2A5). The number of back-labeled PVN GFP (exclusively OT) neurons was comparable (33.4 ± 9.1) with the estimation by non-selectively labeled PVN neurons identified by co-staining with OT antibodies.

OT neurons similar in morphology and location were obtained in our initial study (data not shown) with the application of latex retrobeads (Katz and Iarovici, 1990)

in the SON, which, however, labeled only few cells in the PVN (and other structures innervating the SON; Figure S3), precluding quantitative analysis.

We determined the electrophysiological characteristics of fluorescently labeled neurons in the PVN to assess their parvocellular nature. We conducted whole-cell patch clamp recordings in slices (Figure 2B) in current clamp applying a protocol of depolarizing current injections (Figure 2B1). This was aimed to determine the presence of a transient outward rectification which is typically found in magnOT, but not in parvOT neurons (Lüther et al., 2002). We recorded in a total of 7 animals 11 fluorescent putative parvOT, and found that none, as expected, exhibited a hyperpolarizing notch. Conversely, all of the 13 non-fluorescent neurons from the same region (putative magnOT) showed the typical transient outward rectifying current, aka "notch". Quantification of these differences was made by analyzing the time to spike (spike delay) and rise slope which was the slope measured between beginning of the depolarization and the peak time of the first action potential. Both of these parameters showed highly significant differences between the two groups of neurons (Table S4; Figure S4). Differences in the spike frequency also showed a tendency though with less significance than previously reported (Lüther et al., 2000). The electrophysiological responses were in agreement with the morphology of the cells. Neurons classified electrophysiologically as parvOT had a small soma and a more elongated shape, while the ones classified as magnOT had a big soma and were more rounded (Figure 2B).

ParvOT Neurons Innervating MagnOT Neurons Also Project Specifically to

NK1R/OTR Positive WDR Neurons in the Deep Layers of the SC.

The above established exclusive labeling of parvOT neurons and all their processes using a combination of CAV2-Cre with OT cell typed-specific Cre-dependent rAAV (Figure 3A1-A3) allowed us to follow projections of this OT cell population up to the distal (L5) segments of the SC. After labeling presumably all PVN OT neurons, axons can be visualized in both superficial and deep spinal cord layers (Figure S5A). In contrast, we found that synaptophysin-GFP-filled terminals from parvOT only were loosely and sparsely distributed in superficial laminae, but heavily innervate deep laminae, in close proximity to neurokinin 1 receptor (NK1R)-positive large cells (diameter 30-40 µm; Figure 3A2) identified as sensory wide dynamic range (WDR) neurons (Ritz and Greenspan, 1985). Importantly, in an additional labeling (on separate slices because both OTR and NK1R antibodies had been raised in the same species) we found in this same region cells that expressed OT receptors (OTR, Figure 3A3). The specificity of the antibody was confirmed in transfected HEK cells (Figure S5B1) and brainstem sections of OTR knockout mice (Figure S5B2), in agreement with a previous study using these antibodies in mouse cortex (Marlin et al., 2015). To show the colocalization of NK1R and OTR in the same cells we performed fluorescent *in situ* hybridization and found the presence of respective mRNAs in same neurons of deep layers of the SC (Figure 3B1-B4). As a next step, we wanted to demonstrate that NK1R-positive neurons of deep SC laminae could be activated by sensory/pain stimulation. Bilateral injection of capsaicin in the hindpaws indeed induced c-Fos expression in large NK1R neurons (Figure 3C1-

C3). Furthermore, back-labeled parvOT neurons were also activated by capsaicin (not shown).

To show that NK1R WDR neurons are functionally modulated by both NK1R specific agonist (SarMet-SP) and parvOT-deriving OT, we measured *in vivo* the WDR C-fiber evoked spikes in response to a series of isolated hindpaw stimulations. We found that the C-fiber evoked spikes were increased in the presence of SarMet-SP, as expected (Budai and Larson, 1996). Interestingly, BL-activation of ChR2 expressing parvOT fibers in the SC (SC-BL; schemes in Figure 5A-B) upon SarMet-SP significantly reduced the number of C-fiber evoked spikes from 16.8 ± 1.1 to 11.2 ± 1.5 (Figure 3D1-D2). These findings show that release of OT from parvOT axons can effectively inhibit the activity of WDR neurons potentiated by NK1R activation.

Then, we analyzed the inhibitory effect of OT on WDR neuron firing properties. To do so, we performed *in vitro* whole-cell patch clamp recordings in current clamp applying a protocol of depolarizing current injections (Figure 3E; Breton et al., 2009). Putative WDR neurons, identified by their large cell body and repetitive firing related to stimulation intensities (Figure 3E; Ritz and Greenspan, 1985), were located around the central canal (cc) and in deep layers V-VI. As expected, TGOT was able to change the firing properties of these neurons, from repetitive to phasic in 5/9 of recorded cells (Figure 3E), similar to what was described in superficial layers (Breton et al., 2009). Importantly, the application of specific biased agonist for OTR linked to G_i subunit, Atosiban (Busnelli et al., 2012), induced the exact same effects in 4/7 recorded cells (Figure 3E). This

experiment demonstrates for the first time on living tissue that OTR can functionally bind a G_i protein, thus elucidating the inhibitory mechanism of OT on the firing properties of WDR neurons.

Finally, to demonstrate that the population of identified parvOT neurons is a single anatomical unit and that the same cells project collaterals to both the SON and SC, we injected CAV2 virus in deep laminae of L5, and Cre-responder AAV expressing GFP under the OT promoter in the PVN (Figure 4A1). We detected back-labeled cell bodies of GFP/OT neurons in the PVN and their axonal projections in close proximity to somas and dendrites of magnOT neurons of the SON (Figure 4A2-A5).

ParvOT Neurons Projecting to MagnOT SON Neurons and NK1R/OTR Positive WDR Neurons in Deep Layers of the SC Control the Central Nociceptive Processing.

To test whether the specific population of PVN-OT neurons projecting to both the SON and SC indeed acts on nociceptive input, we recorded SC neuronal responses *in vivo* during electrical stimulation of their hindpaw receptive field. The coding properties and short-term potentiation (wind-up; WU) following repetitive receptive field stimulation were calculated from the response of WDR neurons in deep laminae. Recordings include the deep laminae, which integrate convergent peripheral sensory information from fast-conducting (A-type) and slow-conducting (C-type) primary afferent fibers (Figure 5 and S6).

We first tested the inhibitory action of OT released from parvOT-hypothalamo-spinal terminals by shining BL directly onto the dorsal surface of the SC (SC-BL). In this set of experiments, we used the same combination of viruses (CAV2-Cre and rAAV carrying OT promoter-DIO-ChR2-mCherry) to elicit OT release from parvocellular PVN fibers. SC-BL efficiently reduced the WDR discharges from C- (-44.6 ± 3.7 %; Figure 5C1-C2) and Aδ- (-36.3 ± 4.5 %), but not from Aβ- fibers (-0.3 ± 2.8 %; Figure S6G2). The half-efficacy of SC-BL inhibition was 8.3 ± 1.3 s (Figure 5E). The WU returned to control values ~300 s after SC-BL (Figure 5C1). SC-BL had no effect on superficial layer neuron activity in the same recording condition as for WDR neurons (Figure S6F). The OTR antagonist dOVT, directly applied to the surface of the SC, significantly but not entirely reduced Aδ- and C-fiber mediated discharges (Figure 5C1-C2). In contrast, the vasopressin receptor type 1A antagonist applied on SC failed to change the SC-BL inhibition of WU intensity (Figure 5C2) whereas it could efficiently block the effect of exogenously applied AVP (not shown). Since VGluT2 was detected in synaptophysin-GFP-containing (Figure 5F1-F2; overlap of GFP and vGluT2 signals was found is 89 ± 7.4 % GFP terminals) axonal terminals of parvOT neurons near cell bodies of WDR-like neurons (Figure 5F2) we assessed the effect of NBQX *in vivo*. Co-application of both dOVT and NBQX entirely blocked the SC-BL effects (Figure 5C1-C2). Thus, stimulation of parvOT axons in SC deep layers leads to a fast, short-lasting decrease in nociceptive processing which is mediated by central OTR, and to a lesser extent by ionotropic Glut receptors.

We then assessed the efficiency of OT release from parvOT neurons onto magnOT SON neurons in modulating nociception (Figure 5B and S6A). Eliciting

OT release from parvOT fibers in SON by blue light (SON-BL) significantly reduced the WDR discharges evoked by slow-conducting C-type fibers (-24.9 ± 3.1 %; Figure 5D1 and 5D2) and fast-conducting fibers Aδ- (-30.0 ± 6.8 %), but not by non-nociceptive, fast-conducting Aβ- fibers (-6.4 ± 3.5 %; Figure S6G1). The half-efficacy of SON-BL induced inhibition of WU was 22.2 ± 3 s (T 50 %, Figure 5E), a value which was significantly higher than the SON-BL effect (Figure 5E). The WU intensity returned to control values only 800 s after SON-BL (Figure 5D1). Moreover, to further confirm that the reduction in WU intensity was related to the elevated level of blood OT (see Figure 1E), we injected the OT receptor (OTR) antagonist dOVT intravenously before applying SON-BL. As expected, this abolished the SON-BL inhibition of WDR discharges that were evoked by both Aδ- and C-fibers (Figure 5D1-D2 and S6G1). Thus, the central release of OT from parvOT axons targeting magnOT SON neurons leads to a systemic release of OT, which reduces nociceptive processing by WDR neurons. This effect was slow to appear and long-lasting.

In summary, the subpopulation of PVN OT parvOT neurons projecting both to magnOT SON neurons and to NK1R/OTR WDR neurons from deep layers of SC exerts an inhibition of spinal nociceptive processing by fast action on SC neurons and a relatively slower effect on peripheral targets by stimulation of SON neurons and subsequent induction of OT release into blood.

Activation of ParvOT Neurons Results in Analgesia

In the last part of our work we analyzed the functional importance of these

parvOT neurons in the processing of inflammatory compared to nerve injury-induced neuropathic pain. To this purpose, we measured both the effects of stimulation or inhibition of parvOT neurons on the symptoms of either a peripheral painful inflammatory sensitization triggered by a single unilateral intraplantar injection of complete Freund adjuvant (CFA) or a nerve injury-induced neuropathy induced by the cuffing of the sciatic nerve (Cuff, Pitcher et al., 1999; Figure S7C1). To this purpose we used rats that expressed either ChR2 or hM4Di (Zhu and Roth, 2014) restricted to parvOT PVN neurons synapsing on magnOT SON neurons (Figure 6A). The efficiency of ChR2-mediated activation and hM4Di-mediated inhibition of OT neurons was assessed respectively by the BL targeting unilaterally the PVN or CNO *i.p.* administrated and was confirmed both *in vitro* (Figure S7A1-A2) and *in vivo* (Figure S7B1-B4).

PVN-BL stimulation significantly, but not entirely, alleviated the CFA-mediated hyperalgesia by raising the threshold of response to both the mechanical (from 56.7 ± 7.6 g to 116.6 ± 16.4 g) and thermal hot stimulation (from 2.8 ± 0.2 to 4.8 ± 0.7 s; Figure 6C1-C2). In contrast, PVN-BL failed to mitigate the mechanical hyperalgesia measured in condition of the Cuff peripheral neuropathy (Figure S7B2-B3). Furthermore, return of the pain symptoms occurred after PVN-BL was fully blocked by intraperitoneal injection of the blood brain barrier (BBB)-permeable OTR antagonist L-368,899 (Figure 6C1-C2).

Conversely, CNO-induced inhibition of parvOT neurons significantly increased the CFA-mediated hyperalgesia by lowering the threshold of response to both the mechanical (from 115 ± 12.1 g to 88 ± 9.8 g) and thermal hot stimulation (from

8.1 ± 0.9 s to 6.3 ± 0.3 s; Figure 6C1-C2). CNO had no effect in rats with the Cuff (Figure S7C2-C3). These results from gain- and loss-of-function approaches highlight the role of parvOT control of peripheral painful sensitization, supported by our *in vivo* electrophysiological data.

In the course of our study we observed that both PVN-BL and CNO failed to modify mechanical and thermal hot sensitivity in the absence of any peripheral sensitization, *i.e.* in the contralateral paw or in naïve animals (Figure 6B1-B2 and 6C1-C2 and S7C2-C3).

Taken together, these findings provide evidence that thirty parvOT neurons are able to strongly promote analgesia in a pathological condition of inflammatory, but not nerve injury-induced neuropathic pain, presumably by both central (SC-mediated) and peripheral (SON-mediated) mechanisms.

DISCUSSION

Here we identified, by a combination of latest state of the art viral-vector based (Grinevich et al., 2016), anatomical, optogenetic, electrophysiological, and behavioral approaches, a small (n ~30) subpopulation of parvOT neurons in the PVN, which projects to magnOT neurons in the SON and to NK1R or OTR-positive WDR neurons in the deep layers of the SC. Functionally, we demonstrated that this network can inhibit spinal pain processing in a dual manner with two distinct time courses. Thus, nociceptive transmission from Aδ- and C-type primary afferents to WDR neurons is efficiently repressed by OT release from parvOT in the deep layers of the SC and from SON magnOT in the blood. Release in the SC is directly triggered from parvOT-spinal projections and follows a fast mode of action; release in the blood is indirectly triggered from SON magnOT neurons that are activated by parvOT projections and follows a slower time course. The functional role of this subpopulation of parvOT neurons was further confirmed in two rat models of peripheral painful sensitization, indicating that activation of parvOT neurons can decrease mechanical and thermal sensitivities in inflammatory but not nerve injury-induced neuropathic pain.

Synaptic Cross-Talk Between OT Neurons

The question of how OT neurons in different nuclei within the hypothalamus interact with each other is a recurrent theme in past literature, but has not been elucidated experimentally. Belin and colleagues recorded pairs of OT neurons from SON and PVN and proposed an internuclear connection serving as a basis for synchronous firing during lactation (Belin et al., 1984, Belin and Moos, 1986).

The hypothesis of an OT-mediated communication was stated already in the early 80's (Silverman et al., 1981) following observations that application of OT (or dOVT) into the third ventricle or in the SON synchronized (respectively desynchronized) activity of OT neurons in PVN and SON (Freund-Mercier and Richard, 1984; Lambert et al., 1993). Furthermore, the presence of synapses containing OT-immunoreactivity was demonstrated in the SON (Theodosis, 1985). Although we did not examine internuclear connectivity that underlies synchronized burst firing, our anatomical and functional data demonstrate that PVN-SON interconnectivity plays an important role in inhibiting spinal nociceptive processing and alleviation of inflammatory pain.

In an early study, lesion of the SON did not cause any loss of magnOT neurons in the PVN (Olivecrona, 1957), providing a first indication that parvOT PVN neurons might be at the basis of internuclear connection to the SON. However, as of today, the parvOT neurons in the PVN have remained much less studied than the magnOT neurons, mostly because of technical difficulties, specifically in labeling and modulating the activity of parvOT neurons. To our knowledge, the possibility to study a direct parvOT innervation of the SON by retrograde tracing techniques has seldom been discussed (*e.g.* Lambert et al., 1993), and any potentially involved parvocellular neurons have never been identified.

At the SON level, Bruni and Perumal (1984) have described an extensive network of small-diameter, beaded, unmyelinated fibers with no particular organizational pattern and of unknown origin that establishes functional axo-somatic and axo-dendritic contacts with magnOT neurons. Thirty years later, we

reveal here a monosynaptic connection between parvOT PVN and magnOT SON neurons as respective pre- and postsynaptic components. The detection of a postsynaptic SON component was further confirmed by their stimulation through application of CCK (Renaud et al., 1987) and an increase in peripheral OT levels.

In contrast to the OT system, direct connectivity between VP-ergic neurons in rats has not been convincingly demonstrated and, accordingly, we were unable to find VP/Venus positive fibers descending the PVN in the SON and vice versa.

ParvOT Neurons modulate NK1R positive WDR neurons

In addition to the control of magnOT activity, this newly described subpopulation of parvOT neurons densely projects exclusively to the deep layers (V, VI, X) of the SC. Axonal terminals from parvOT were found in close appositions with NK1R positive WDR neurons, some of which likely OTR-positive. However, we are not excluding projections of these parvOT neurons to non-WDR deep neurons. Nevertheless, their functional and selective inhibition of C- and Aδ-mediated discharges in WDR suggest that nociceptive C-fiber project to deep layers, accordingly with models of dorsal horn circuits that include projections to the lamina V (Cervero and Connell, 1984; Ribeiro-da-Silva and De Koninck, 2008). Functionally, this fits with our results suggesting that OT modulates the excitability of WDR shown as an inhibition of discharges mediated by fibers containing substance P.

ParvOT Neurons Coordinate Neuroendocrine and Hardwired Inhibitory Pain Control

In accordance with our anatomical data, WDR action potential discharges in response to noxious peripheral stimulation are reduced by optogenetic manipulation of the subpopulation of OT neurons in the PVN and its subsequent stimulation at the level of the SON. This reduction was selective to sensory information transmitted by Aδ- and C-fibers, which are, in their majority, nociceptive-specific.

Regarding peripherally mediated OT effects, it has recently been shown that OTR could be expressed by non-peptidergic C-type sensory neurons in dorsal root ganglia (Moreno-López et al., 2013) and the *in vitro* application of OT suppresses their activity (Gong et al., 2015). Furthermore, intravenous administration of a selective OTR agonist induces an inhibition of discharges mediated by nociceptive-specific primary afferents (Juif et al., 2013). Our present work provides an additional support for this idea by selectively activating a circuit leading to release of OT to the blood (Figure 7). The effect was fully peripheral, since inhibition of nociceptive messages was completely abolished by the addition of the OTR selective antagonist dOVT in the blood flow.

Identification of a subpopulation of parvOT neurons projecting collaterals to both the SON and deep layers of the SC gave rise to the idea that these neurons may exert both a peripheral and central control by OT which we found to take place with a dual time course. This was confirmed by optogenetically-stimulating parvOT PVN axons located either in the SON or in the SC. This stimulation led to a reduction of WDR discharges in response to a peripheral noxious stimulation, which was selective for Aδ- and C-type nociceptive fibers. The effects in deep

layers of the SC seemed to be mediated by the OT receptor as we did not find any effects of VP V1a receptor similar to what has been reported (Qiu et al., 2014). As OT terminals on WDR-like neurons contained VGluT2, we assessed glutamate (Glu) and OT contribution to the SC-BL effect on WU intensity. This revealed that both OT and Glu participated to the inhibition of WU. These results are in accordance with our *in vitro* patch-clamp experiment and can be interpreted by a network effect as OT axons are likely to form en passant synapses (Knobloch et al., 2012), allowing local (micro)volume-transmission from release sites (Grinevich and Knobloch, 2014; Grinevich et al., 2015). The combination of two processes can then explain the observed effects: i) OT acts on OTR in WDR neurons to inhibit them via G_i intracellular pathway (Figure 3E); ii) co-released Glu either activates local GABA-interneurons in layers V-VI and around the central canal (Schneider and Lopez, 2002; Deuchars et al., 2005), which, in turn, inhibit WDR neurons, or binds a mGluR leading to the direct inhibition of WDR neurons by a $G_{i/o}$ pathway (Gerber et al., 2000; Niswender and Conn, 2010).

Surprisingly, evoked spinal OT release by this subpopulation of parvOT did not modify nociceptive processing by neurons in superficial layers. This suggested that the OT inhibition of WDR firing was not induced by OTR activation in superficial layers but only in deep dorsal horn layers. This was in agreement with our anatomical data describing the vast majority of parvOT neurons projecting to the deep layers. We failed to reveal any functional contribution of this subpopulation of parvOT projecting to SON and SC in a nerve-induced neuropathic pain, which may be modulated by OT projections to superficial layers

of the dorsal horn. In contrast, they exerted a tonic inhibitory control on WU and pain symptoms in the peripheral inflammation. We speculate that the inflammatory component in pain state regulates the excitability of this subset of parvOT neurons, as demonstrated by c-Fos induction in parvOT neurons in Figures S2. Our results indicate that the described subpopulation of parvOT neurons specifically targets NK1R and OTR positive neurons located in the deep layers of the SC to exert antinociceptive action on WDR to promote analgesia.

Described ParvOT Neurons as a New OT-ergic Cell Type

Following pioneering works of Sawchenko, Swanson and their colleagues (Swanson and Kuypers, 1980; Sawchenko and Swanson, 1982; Swanson and Sawchenko, 1983), parvOT neurons have been considered as heterogeneous cell populations with descending projections to brainstem and/or SC regions. However, in the present study, we found a small group of parvOT neurons which forms a pathway distinct from the classical hypothalamo-neurohypophyseal axonal tract through the hypothalamus. Although we did not analyze in detail axonal collaterals of these parvOT cells in other forebrain regions, their existence in the hypothalamus adds a new feature to parvOT cells. In addition, these neurons simultaneously project collaterals to deep layers of the SC, representing a unique group of specifically located cells, which is likely distinct from the OT-immunoreactive neurons described by Jojárt et al. (2009) that massively project axons to the superficial layers of the SC. Based on the unique connectivity of the identified parvOT neurons, we speculate that they represent a new type of OT neurons, which coordinate central and peripheral inhibition of nociception and pain perception, and hence, play a role in promoting analgesia (Figure 7).

EXPERIMENTAL PROCEDURES

Animals

Anatomical, electrophysiological, optogenetic and behavioral studies were performed with Wistar rats (for details of the experiment see the respective figure legend). If not mentioned, rats were housed under standard conditions with food and water available *ad libitum*. All experiments were conducted under licenses and in accordance with EU regulations.

Viruses

rAAVs (serotype 1/2) carrying conserved regions of OT and VP promoters and genes of interest in direct or "floxed" orientations were cloned and produced as reported previously (Knobloch et al., 2012). CAV2 equipped either with Cre recombinase was purchased from Institute of Molecular Genetics in Montpellier CNRS, France (Bru et al., 2010)

Neuroanatomy

To trace inter-nuclear connections rAAVs expressing Venus were injected into the PVN or SON to follow their axonal projections within the hypothalamus. Alternatively, CAV2-Cre was injected into the SON, while Cre-dependent "floxed" rAAV – into the PVN to identify OT PVN neurons synapsing onto SON neurons.

To trace hypothalamus-spinal cord connections, CAV2-Cre virus was injected into the SON and "floxed" rAAV – into the PVN or CAV2-Cre virus was injected in the spinal cord, while Cre-dependent rAAV – into the PVN. This allowed to visualize OT axon pattern in the spinal cord and to identify projecting PVN OT

neurons, respectively. After transcardial perfusion with 4% PFA, brains and/or spinal cords were sectioned and stained with antibodies against OT, VP, vGluT2, GFP, NeuN, NK1R, and OTR. Images for qualitative and quantitative analyses were taken on confocal microscopes Leica SP2 and SP5.

Electrophysiology Experiments

For *in vitro* patch-clamp recordings, four-to-eight weeks after injection of virus in adult rats, brains were removed, the hypothalamus or lumbar spinal cord was isolated, cut into 400 µm coronal slices, and kept in artificial cerebrospinal fluid (ACSF: 118 mM NaCl, 25 mM NaHCO3, 10 mM glucose, 2 mM KCl, 2 mM MgCl2*6H2O, 2 mM CaCl2*2H2O, 1.2 mM NaH2PO4) saturated 95% O2, 5% CO2. Visualized neurons were patched with borosilicate glass pipette (4-9 MΩ) filled with 140 mM KMeSO4, 10 mM HEPES, 2 mM MgCl2, 0.1 mM CaCl2, 0.1 mM BAPTA, 2 mM ATP Na salt, 0.3 mM GTP Na salt (pH 7.3), adjusted to 300 mOsm and voltage-clamped at -60 mV.

For *in vivo* extracellular recordings, four-to-eight weeks after injection of virus, in adult animals were anaesthetized with 4% isoflurane and placed in stereotaxic frame. Extracellular neuronal activity was recorded using a stainless electrode with 10MΩ impedance (FHC, USA; UE(FK1)).

Behavioral Experiments

Mechanical allodynia was measured using a calibrated forceps (Bioseb, Chaville, France). Thermal allodynia/hyperalgesia was measured using the Plantar test using Hargeaves method (Ugo Basile, Comerio, Italy). Peripheral painful inflammatory sensitization was obtained by a single unilateral intraplantar

injection of complete Freund adjuvant (Sigma-Aldrich, 100 µl in the right paw). Nerve injury-induced neuropathy was induced by the cuffing of the sciatic nerve.

SUPPLEMENTAL INFORMATION

Supplemental Information includes Conflict of Interest Disclosure, Supplemental Experimental Procedures, three tables and six figures and can be found with this article online.

REFERENCES

Armstrong, W.E., Warach, S., Hatton, G.I., and McNeill, T.H. (1980). Subnuclei in the rat hypothalamic paraventricular nucleus: a cytoarchitectural, horseradish peroxidase and immunocytochemical analysis. Neuroscience *5*, 1931–1958.

Atasoy, D., Betley, J.N., Su, H.H., and Sternson, S.M. (2012). Deconstruction of a neural circuit for hunger. Nature. *488*, 172–177.

Bargmann, W., and Scharrer, E. (1951). The site of origin of the hormones of the posterior pituitary. American Scientist *39*, 255–259.

Belin, V., and Moos, F. (1986). Paired recordings from supraoptic and paraventricularoxytocin cells in suckled rats: recruitment and synchronization. J. Physiol. (Lond). *377*, 369–390.

Belin, V., Moos, F., and Richard, P. (1984). Synchronization of oxytocin cells in the hypothalamic paraventricular and supraoptic nuclei in suckled rats: direct proof with paired extracellular recordings. Exp. Brain Res. *57*, 201–203.

Ben-Barak, Y., Russel, J.T., Whitnall, M.H., Ozato, K., and Gainer, H. (1985). Neurophysin in the hypothalamo-neurohypophyseal system. I. Production and characterization of monoclonal antibodies. J. Neurosci. *5*, 81–97.

Boudaba, C., and Tasker, J.G. (2006). Intranuclear coupling of hypothalamic magnOT nuclei by glutamate synaptic circuits. Am. J. Physiol. Regul. Integr. Comp. Physiol. *291*, R102–R111.

Bru, T., Salinas, S., and Kremer, E.J. (2010). An update on canine adenovirus type 2 and its vectors. Viruses *2*, 2134–2153.

Bruni, J.E., and Perumal, P.M. (1984). Cytoarchitecture of the rat's supraoptic nucleus. Anat. Embryol. *170*, 129–138.

Budai, D, and Larson, A.A. (1996). Role of substance P in the modulation of C-fiber evoked responses of spinal dorsal horn neurons. Brain Res. *710*, 197-203.

Busnelli, M., Saulière, A., Manning, M., Bouvier, M., Galés, C., Chini, B. (2012) Functional selective oxytocin-derived agonists discriminate between individual G protein family subtypes. J Biol Chem 287(6):3617-29

Condés-Lara, M., González, N.M., Martínez-Lorenzana, G., Delgado, O.L., and Freund-Mercier, M.J. (2003). Actions of oxytocin and interactions with glutamate on spontaneous and evoked dorsal spinal cord neuronal activities. Brain Res. *976*, 75–81.

Cunningham, E.T. Jr, and Sawchenko, P.E. (1988). Anatomical specificity of noradrenergic inputs to the paraventricular and supraoptic nuclei of the rat hypothalamus. J. Comp. Neurol. *274*, 60–76.

Deuchars S.A., Milligan C.J., Stornetta R.L., Deuchars J. (2005). GABAergic neurons in the central region of the spinal cord: a novel substrate for sympathetic inhibition. J Neurosci. 25(5):1063-70.

During, M.J., Young, D., Baer, K., Lawlor, P., and Klugmann, M. (2003). Development and optimization of adeno-associated virus vector transfer into the central nervous system. Meth. Mol. Med. *76*, 221–236.

Dölen, G., Darvishzadeh, A., Huang, K.W., and Malenka, R.C. (2013). Social reward requires coordinated activity of nucleus acumbens oxytocin and serotonin. Nature *501*, 179–184.

Freund-Mercier, M.J., and Richard, P. (1984). Electrophysiological evidence for facilitatory control of oxytocin neurones by oxytocin during suckling in the rat. J. Physiol. (Lond). *352*, 447–466.

Gerber G, Zhong J, Youn D, Randic M. (2000) Group II and group III metabotropic glutamate receptor agonists depress synaptic transmission in the rat spinal cord dorsal horn. Neuroscience. *100(2)*:393-406.

Gong, L., Gao, F., Li, J., Li, J., Yu, X., Ma, X., Zheng, W., Cui, S., Liu, K., Zhang, M., Kunze, W., Liu, C.Y. (2015). Oxytocin-induced membrane hyperpolarization in pain-sensitive dorsal root ganglia neurons mediated by Ca(2+)/nNOS/NO/KATP pathway. Neuroscience. *289,* 417–428.

González-Hernández, A., Rojas-Piloni, G., and Condés-Lara M. (2014). Oxytocin and analgesia: future trends. Trends Pharmacol. Sci. *35*, 549–551.

Grinevich, V., Knobloch, H. S., Roth, L.C., Althammer, F., Domansky, A., Vinnikov, I., Stanifer, M., and Boulant, S. (2015). Somatic transgenesis (Viral vectors). *Molecular Neuroendocrinology: From Genome to Physiology,* First Edition. Edited by David Murphy and Harold Gaine*r.* John Wiley & Sons, Ltd. 2016, pp. 243 – 274.

Grinevich, V., Knobloch-Bollmann, H.S., Eliava, M., Busnelli, M., Chini, B. (2015): Assembling the puzzle: Pathways of oxytocin signaling in the brain. Biol. Psychiatry, in press. doi:10.1016/j.biopsych.2015.04.013

Hargreaves, K., Dubner, R., Brown, F., Flores, C., Joris, J. (1988). A new and sensitive method for measuring thermal nociception in cutaneous hyperalgesia. Pain *32*, 77–88.

Jójárt, I., Boda, K., Gálfi, M., Mihály, A., B-Baldauf, Z., and Vecsernyés, M. (2009). Distribution of oxytocin-immunoreactive neuronal elements in the rat

spinal cord. Acta Biol Hung. *60*, 333–346.

Juif, P.E., Breton, J.D., Rajalu, M., Charlet, A., Goumon, Y., and Poisbeau, P. (2013). Long-lasting spinal oxytocin analgesia is ensured by the stimulation of allopregnanolone-like neurosteroid synthesis which potentiates GABAA receptor-mediated synaptic inhibition. J. Neurosci. *33*, 16617–16626.

Juif, P.E, and Poisbeau, P. (2013). Neurohormonal effects of oxytocin and vasopressin receptor agonists on spinal pain processing in male rats. Pain *154,* 1449–1456

Katz, L.C., and Iarovici, D.M. (1990). Green fluorescent latex microspheres: a new retrograde tracer. Neuroscience *34*, 511–520

Knobloch, H.S., Charlet, A., Hoffmann, L.C., Eliava, M., Khrulev, S., Cetin, A.H., Osten, P., Schwarz, M. K., Seeburg, P.H., Stoop, R., and Grinevich, V. (2012). Evoked axonal oxytocin release in the central amygdala attenuates fear response. Neuron *73*, 553–566.

Lambert, R.C., Moos, F.C., and Richard, P. (1993). Action of endogenous oxytocin within the paraventricular or supraoptic nuclei: a powerful link in the regulation of the bursting pattern of oxytocin neurons during the milk-ejection reflex in rats. Neuroscience *57*, 1027–1038.

Lee, H.-J., Pagani, J., and Young, W.S., III (2010). Using transgenic mouse

models to study oxytocin's role in the facilitation of species propagation. Brain Res. *1364*, 216–224.

Luis-Delgado, O.E., Barrot, M., Rodeau, J.L., Schott, G., Benbouzid, M., Poisbeau, P., Freund-Mercier, M.J., and Lasbennes, F. (2006). Calibrated forceps: a sensitive and reliable tool for pain and analgesia studies. J. Pain *7*, 32–39.

Lüther, J.A., and Tasker, J.G. (2000). Voltage-gated currents distinguish parvocellular from magnocellular neurones in the rat hypothalamic paraventricular nucleus. J. Physiol. 523, 193–209.

Lüther, Jason A., Katalin Cs. Halmos, and Jeffrey G. Tasker. A slow transient potassium current expressed in a subset of neurosecretory neurons of the hypothalamic paraventricular nucleus. J Neurophysiol 84: 1814–1825, 2000

Luther, J.A., Daftary, S.S., Boudaba, C., Gould, G.C., Halmos, K.C., and Tasker, J.G. (2002). Neurosecretory and non-neurosecretory parvocellular neurons of the hypothalamic paraventricular nucleus express distinct electrophysiological properties. J. Neuroendocrinol. *14*, 929–932.

Mack, S.O., Kc, P., Wu, M., Coleman, B.R., Tolentino-Silva, F.P., and Haxhiu, M.A. (2002). Paraventricular oxytocin neurons are involved in neural modulation of breathing. J. Appl. Physiol. *92*, 826–834.

Marlin, B.J., Mitre, M., D'amour, J.A., Chao, M.V., and Froemke, R.C. (2015). Oxytocin enables maternal behaviour by balancing cortical inhibition. Nature *520*, 499–504.

Martínez-Lorenzana, G., Espinosa-López, L., Carranza, M., Aramburo, C., Paz-Tres, C., Rojas-Piloni, G., and Condés-Lara, M. (2008) PVN electrical stimulation prolongs withdrawal latencies and releases oxytocin in cerebrospinal fluid, plasma, and spinal cord tissue in intact and neuropathic rats. Pain 140, 265–273.

Mendell, L.M., and Wall, P.D. (1965). Responses of single dorsal cord cells to peripheral cutaneous unmyelinated fibers. Nature *206*, 97–99.

Miselis, R.R. (1981). The efferent projections of the subfornical organ of the rat: a circumventricular organ within a neural network subserving water balance. Brain Res. *230*, 1–23.

Moos, F., and Richard, P. (1989). Paraventricular and supraoptic bursting oxytocin cells in rat are locally regulated by oxytocin and functionally related. J. Physiol. (Lond). *408*, 1–18.

Moreno-López, Y., Martínez-Lorenzana, G., Condés-Lara, M., and Rojas-Piloni, G. (2013). Identification of oxytocin receptor in the dorsal horn and nociceptive dorsal root ganglion neurons. Neuropeptides. *47*, 117–123

Nagel, G., Szellas, T., Huhn, W., Kateriya, S., Adeishvili, N., Berthold, P., Ollig, D., Hegemann, P., and Bamberg, E. (2003). Channelrhodopsin-2, a directly light-gated cation-selective membrane channel. Proc. Natl. Acad. Sci. USA *100*, 13940–13945.

Neher, E. (1992). Correction for liquid junction potentials in patch clamp experiments. Methods Enzymol. *207*,123–131.

Niswender, C.M., Conn, J. (2010). Metabotropic Glutamate Receptors: Physiology, Pharmacology, and Disease. Annu Rev Pharmacol Toxicol 50:295-322.

Olivecrona, H. (1957). Paraventricular nucleus and pituitary gland. Acta Physiol. Scand. S*40*, 1–178.

Paxinos, G., and Watson, C. (1998). The Rat Brain in Stereotaxic Coordinates, Fourth Edition (London: Academic Press).

Petersson, M. (2002). Cardiovascular effects of oxytocin. Prog. Brain Res. *139*, 281–288.

Pitcher, G. M., Ritchie, J., Henry, J. L. (1999). Nerve constriction in the rat: model of neuropathic, surgical and central pain. Pain 83(1):37-46.

Qiu, F., Qiu, C.Y., Cai, H., Liu, T.T., Qu, Z.W., Yang, Z., Li, J.D., Zhou, Q.Y, and Hu, W.P. (2014). Oxytocin inhibits the activity of acid-sensing ion channels through the vasopressin, V1A receptor in primary sensory neurons. Br. J. Pharmacol. *171*, 3065–3076.

Renaud, L.P., Tang, M., McCann, M.J., Stricker, E.M., and Verbalis, J.G. (1987). Cholecystokinin and gastric distension activate oxytocinergic cells in rat hypothalamus. Am. J. Physiol. *253*, R661–R665.

Reiter, M.K., Kremarik, P., Freund-Mercier, M.J., Stoeckel, M.E., Desaulles, E., and Feltz, P. (1994). Localization of oxytocin binding sites in the thoracic and upper lumbar SC of the adult and postnatal rat: a histoautoradiographic study. Eur. J. Neurosci. *6*, 98–104.

Ribeiro-da-Silva A, De Koninck Y (2008). Morphological and neurochemical organization of the spinal dorsal horn. In: Basbaum AI, Bushnell MC, editors. Science of Pain. Elsevier.

Ritz, L.A., and Greenspan, J.D. (1985). Morphological features of lamina V neurons receiving nociceptive input in cat sacrocaudal spinal cord. J. Comp. Neurol. *4*, 440-452.

Ross, H.E., Cole, C.D., Smith, Y., Neumann, I.D., Landgraf, R., Murphy, A.Z., and Young, L.J. (2009). Characterization of the oxytocin system regulating affiliative behavior in female prairie voles. Neuroscience *162*, 892–903.

Sawchenko, P.E., and Swanson, L.W. (1982). Immunohistochemical identification of neurons in the paraventricular nucleus of the hypothalamus that project to the medulla or to the spinal cord in the rat. J. Comp. Neurol. *205*, 260–272.

Scharrer, E. (1928). Die Lichtempfindlichkeit blinder Elritzen (Untersuchungen über das Zwischenhirn der Fische). Z. vergl. Physiol. *7*, 1–38.

Scharrer, E., and Scharrer, B. (1940). Secretory cells within the hypothalamus. Res. Publ. Ass. nerv. ment. Dis. *20*, 170–194.

Schneider S.P., Lopez M. (2002). Immunocytochemical localization of glutamic acid decarboxylase in physiologically identified interneurons of hamster spinal laminae III-V. Neuroscience. 115(2):627-36.

Schouenborg, J. (1984). Functional and topographical properties of field potentials evoked in rat dorsal horn by cutaneous C-fibre stimulation. J. Physiol. (Lond). *356*, 169 –192.

Silverman, A.J., Hoffman, D.L., and Zimmerman, E.A. (1981). The descending afferent connections of the paraventricular nucleus of the hypothalamus (PVN). Brain Res. Bull. *6*, 47–61.

Sofroniew, M.V. (1983). Morphology of vasopressin and oxytocin neurones and their central and vascular projections. Prog. Brain Res. *60*, 101–114.

Swanson, L.W., and McKellar, S. (1979.) The distribution of oxytocin- and neurophysin-stained fibers in the spinal cord of the rat and monkey. J. Comp. Neurol. *188*, 87–106.

Swanson, L.W., and Kuypers, H.G. (1980). The paraventricular nucleus of the hypothalamus: cytoarchitectonic subdivisions and organization of projections to the pituitary, dorsal vagal complex, and spinal cord as demonstrated by retrograde fluorescence double-labeling methods. J. Comp. Neurol. *194*, 555–570.

Swanson, L.W., and Sawchenko, P.E. (1983). Hypothalamic integration: organization of the paraventricular and supraoptic nuclei. Ann. Rev. Neurosci. *6*, 269–324.

Schwartz, L.A., Miyamichi, K, Gao, X.J., Beier, K.T., Weissbourd, B., DeLoach, K.E., Ren, J., Ibanes, S., Malenka, R.C., Kremer, E.J., Luo, L. (2015). Viral-genetic tracing of the input-output organization of a central noradrenaline circuit. Nature. *524*, 88–92.

Theodosis, T. (1985) Oxytocin-immunoreactive terminals synapse on oxytocin neurones in the supraoptic nucleus. Nature *313, 682-684*.

Verbalis, J.G., McCann, M.J., McHale, C.M., and Stricker, E.M. (1986). Oxytocin secretion in response to cholecystokinin and food: differentiation of nausea from satiety. Science *232*, 1417–1419.

Yang, Q., Wu, Z.Z., Li, X., Li, Z.W., Wei, J.B., and Hu, Q.S. (2002). Modulation by oxytocin of ATP-activated currents in rat dorsal root ganglion neurons. Neuropharmacology 43, 910–916.

Zhu H., Roth B.L. (2014). Silencing synapses with DREADDs. Neuron 82(4):723-5.

Author Contributions

Conceptualization, AC and VG; Methodology, PP, PHS, RSt, AC and VG; Formal Analysis, ME, MMe, HSK-B, JW and AC; Investigation – Neuroanatomy, ME, HSK-B, MdSG, LCR, FA, TG, MB, MMi and GG; Investigation – *In vivo* Electrophysiology, MMe, JW, YT and NP-D; Investigation – *In vitro* Electrophysiology JW, ACC and RTdR; Investigation – Behavior, MMe, JW, MdSG, NP-D and LLT; Investigation – LC-MS/MS, VC any YG; Resources, BC, RCF, MVC, RSp, RK; Writing – Original Draft, MMe, HSK-B, JW, PP, PHS, RSt, AC and VG; Writing – Review & Editing, ME, MMe, HSK-B, JW, PP, PHS, RSt, AC and VG; Visualization, ME, MMe, HSK-B, JW, AC and VG; Supervision, AC and VG; Project Administration, RSt, AC and VG; Funding Acquisition, AC and VG.

Acknowledgements

This work was supported by Chica and Heinz Schaller Research Foundation, German Research Foundation (DFG) grant GR 3619/4-1, Human Frontiers Science Program RGP0019/2015, DFG within the Collaborative Research Center (SFB) 1134 (to VG) and 1158 (to VG and RK) and PHC PROCOP program 32975SA (DAAD and Campus France) (to VG and AC), the IASP Early Career Research grant 2012, FP7 Career Integration grant 334455, Initiative of Excellence (IDEX) Attractiveness grant W13RAT29, University of Strasbourg Institute for Advanced Study (USIAS) fellowship 2014-15, Foundation Fyssen research grant 2015 (to AC). The authors thank Judith Müller, Elke Lederer and Heike Böhli for cloning and packaging viral vectors, Natalie Landeck and Ali

Cetin for the selection of the VP promoter, Anna Illarionova for cloning Cre-depended rAAVs, Scott Sternson for ChR2-mCherry construct, Jonathan Fadok for canine virus, Ulrich Herget and Annemarie Scherbarth for their help with confocal and light-sheet microscopy, Marianna Leonzino for help with the HEK293 experiments, Claudia Pitzer and the Interdisciplinary Neurobehavioral Core for behavioral experiments performed there, Vincent Lelièvre and Pascal Darbon for useful inputs to physiological experiments, Thomas Splettstoesser (SciStyle; www.scistyle.com) for his help with the preparation of Figure 7 and Anne Seller for proof reading the manuscript.

FIGURE LEGENDS

Figure 1. Anatomical and functional connectivity between OT neurons of the PVN and SON

(**A**) OT projections from PVN to SON. (**A1**) Scheme of the viral vector used to infect PVN neurons. (**A2**) PVN OT neurons infected with cell-type specific viral vector project Venus-positive axons to contralateral PVN (**A3**) and to contra- and ipsilateral SON (**A4**, **A5**). OT neurons of the SON (**A6**) do not project Venus axons to contralateral SON (**A7**) or PVN (**A8**) and only marginally enter the external border of ipsilateral PVN (**A9**). Scale bars: left 200 µm; right 50 µm.

(**B**) OT axon terminals contain vGluT2. (**B1**) Scheme of viral vector. (**B2**) GFP-positive terminals in the area of the SON (left panel). In magnified inset (right panel) OT neuron (blue) is surrounded by GFP terminals, which also contain vGlut2 (red). Both immunosignals overlap (yellow) in virtually all terminals. Scale bars: B2 left- 100 µm; B2 right- 25 µm.

(**C**) Electron microscopy OT axon terminals (Venus visualized as DAB endproduct, OT – as a silver-gold-intensified DAB) form asymmetric synapses on OT-ir dendrite within the SON. OT-immunoreactivity (clusters of silver particles, arrows) are shown in the presynaptic axon (a) terminal and postsynaptic dendrite (b) at lower (**C1**) and higher magnifications (**C2**). Scale bar: 0.5 µm.

(**D**) Scheme of the viral vector and setup of *in vivo* electrophysiological recordings (white pipette) in SON, together with SON-BL stimulation (blue fiber) and drug infusion (green pipette). (**D1**-**D3**) Functional connection between PVN and SON OT neurons. (**D1**) Average spike frequencies of SON OT neurons before (Ctrl), after either SON-BL (n=14, blue bar) or systemic injection of CCK

(n=3, yellow bar) and after washout effect (Wash). (**D2**) Relative frequency increase induced by SON-BL in control condition (blue bar), after infusion of NBQX (1uM, 0.5ul; green bar), after additional infusion of dOVT (1uM, 0.5ul; red bar) and after 30 min washout of the drugs (dark blue bar). (**D3**) Histograms of the frequency rates recorded under conditions described in **D2**.

(**E**) Effect of unilateral SON-BL effect on OT blood concentration at the end of SON-BL, 1 min and 30 min after (n=4).

Statistical significances: **++** $p<0.01$, Wilcoxon's test. **o** $p<0.05$, Friedman's test followed by Dunn post-hoc test. Blue squares represent 20 s BL stimulation at 30 Hz with 10ms pulses of BL stimulation.

Figure 2. Anatomical and electrophysiological characteristics of PVN OT neurons projecting to the SON

(**A**) Identification of a subset of OT neurons projecting from PVN to SON. (**A1**) Scheme showing the injection of viruses in the SON and PVN. (**A2, A3**) Defined subset of back-labeled OT neurons (green) in dorso-caudal PVN displays consistent morphology**:** small oval somas (12 to 20 µm in diameter) with predominantly longer horizontal axes. (**A4**) The morphology of these cells is clearly distinct from the typical magnocellular neurons with large cell bodies and less branching processes (**A5**). Scale bar in A2 and A3- 50 µm.

(**B**) Functional differentiation of this subset of PVN OT neurons. (**B1**) Upper trace: Current steps protocol starting from a hyperpolarizing current chosen to reach -100 mV (here 100 pA) followed by progressively more depolarizing current injections. Lower traces: Representative changes in membrane potential for the parvOT and magnOT PVN neurons during the part of the current steps as

indicated by the zoomed area. ParvOT neurons (middle trace) do not display the transient outward rectification specific for the magnOT neurons (lower trace, arrow). (**B2**) Photographs of a GFP-fluorescent parvOT neuron (upper panel) in the PVN (labeled by injection of CAV2-Cre into the SON and OT-DIO-GFP AAV in the PVN) and in the same area a typical magnOT neuron (lower panel) as indicated by the patch pipettes. Scale bars - 20 μm.

Figure 3. ParvOT neurons project to SC and innervate NK1R/OTR WDR neurons in deep laminae

(**A**) ParvOT projections to the SC. (**A1**) Scheme of the viruses injected into the SON and PVN. (**A2**) Detection of synaptophysin-GFP containing terminals (green) in close proximity to NK1R-positive neurons (red) in SC deep laminae. (**A3**) Synatophysin-GFP terminals locate close to OTR-positive neurons of deep laminae. Scale bar in A2, A3- 500 μm.

(**B**) Colocalization of NK1R and OTR mRNAs in the same neurons of SC deep laminae. Immunofluorescent *in situ* hybridization revealed the presence of OTR mRNA (green dots; **B1** and **B4**) and NK1R mRNA (white dots, **B2** and **B4**) in the same neurons, which were visualized by detection of vGlut1/2/3 mRNAs in their somas (pink/violet dots, **B3** and **B4**). Nuclei of cells were stain by DAPI. Arrow heads point NK1R/OTR double positive neurons. Scale bars - 10 μm

(**C**) NK1R- positive SC neurons start to express c-Fos after intraplantar injection of capsaicin in the hindpaw. c-Fos signal (DAB) was detected in deep laminae of SC (**C1**), where NK1R (red) were located (**C2**). Digital overlay of the two signals demonstrates localization of c-Fos in NK1R-postive neuron (**C3**). Scale bars: C1 and C2 – 500 μm; C3 – 50 μm.

(**D**) WDR C-fiber evoked spikes in response to a series of isolated hindpaw stimulations in control condition (Ctrl), during application of the specific agonist of NK1R SarMet-SP (orange), and during SarMet-SP paired with BL (blue). (**D1**) Average of C-fiber evoked spikes (n=5). (**D2**) Representative traces.

(**E**) Discharge profile of putative WDR recorded in current clamp applying a protocol of depolarizing current injections before (black) and after bath application of 1µM TGOT (blue, n=9) or 1µM Atosiban (green, n=7). (**E1**) Proportion of putative WDR neurons discharge pattern changed from repetitive to phasic after TGOT or Atosiban bath application. (**E2**) Example response of putative WDR neuron to 20pA (top), 40pA (middle) and 60pA (bottom) current injection before (black) and after (green) Atosiban bath application. Scale bar: E1- 30µm.

Statistical significance: **o** $p<0.05$, Friedman's test followed by Dunn post-hoc test.

Figure 4. ParvOT-MagnOT-SC Anatomical Unit

(**A**) Scheme of viruses injected into the SC and PVN. The actual SC injection site (fluorescent latex bead accumulation) is shown as an insert undelying SC drawing. (**A2**) PVN parvocellular cells back-labeled from SC (green). GFP-positive cell bodies were found in the caudal portion of the PVN and always co-localized OT (red) (**A3**, magnification from **A2**). Fibers, projecting from back-labeled PVN OT neurons to SON (arrow in **A4**, more caudal to **A2**) GFP-expressing varicouse axons in close proximity to cell bodies and dendrites of SON magnoOT neurons (high magnification in **A5**). Scale bars: A2, A3- 500 µm; A4, A5- 75 µm.

Figure 5. Stimulation of ParvOT PVN Axons in SON and SC Modulates Responses of WDR Neurons

(**A**) Viruses injected into the SON and PVN. (**B**) Scheme of the experimental procedures. (**C**) Effect of SC-BL on WDR-C discharges. (**C1**) Time course of WDR-C in control condition (n=7), when shining SC-BL alone (n=9), after local dOVT application (n=6) or local dOVT + NBQX application (n=6). (**C2**) Average discharge reduction of WDR-C on Ctrl (n=7), when shining SC-BL alone (n=9), after local dOVT application (n=6), local dOVT + NBQX application (n=6) or local V1AR-A application (n=5). Statistical significance of drugs modulation of SON-BL effect was assessed by comparing the effect of SON-BL on the same neuron before and after drug injection. (**D**) Effect of SON-BL on WDR-discharges. (**D1**) Time course of WDR-C in control condition (n=8), measured 30 s after shining SON-BL (as indicated in C1) alone (n=10) or after systemic dOVT systemic injection (n=6). (**D2**) Average discharge reduction of WDR-C on Ctrl (n=8), when shining SON-BL alone (n=10) or after systemic dOVT injection (n=6). Statistical significance of dOVT modulation of SON-BL effect was assessed by comparing the effect of SON-BL on the same neuron before and after dOVT injection (n=6). (**E**) Comparison between individual (black dots) and average T 50 % (blue bar) effect of SON-BL (n=10) and SC-BL (n=7) on recorded WDR.

(**F**) Viruses injected into the SON and PVN. (**F1**, **F2**) Axonal terminals containing synaptophysin-GFP fusion protein in proximity to SC L5 neurons. (**F1**) Overview of fiber distribution within SC: VGluT2 (red), synaptophysin-GFP (green), and NeuN (blue). (**F2**) A zoom in show the green signal (green) largely overlaps with the VGluT2 signal (red) in terminals surrounding cell bodies. Scale bars F1,F2-50 µm.

Statistical significance: ° p<0.05, Friedman with Dunn post-hoc test; **+** p<0.05, **++** p<0.01, Wilcoxon's test; **xx** p<0.01 Kruskal and Wallis test; ****** p<0.01 BL vs. Control, two-ways ANOVA.

Figure 6. Activation/inhibition of Parvocellular OT PVN Neurons Modulates Mechanical Threshold and Thermal Hot Latency in Animals Subjected to Complete Adjuvant Injection

(**A**) (**A1**) Scheme of the experimental procedure. CAV2-Cre was injected in the SON and Cre-responding virus driving either (**A2**) ChR2 or (**A3**) hM4Di to achieve the expression of respective proteins in OT neurons of the PVN.

(**B**) (**B1**) Mechanical thresholds and (**B2**) thermal hot latencies of naïve animals before and after PVN-BL (ChR2, n=6; CNO, n=10).

(**C**) (**C1**) Mechanical thresholds and (**C2**) thermal hot latencies of the CFA-injected hindpaw (left graphs) and the contralateral hindpaw (right graphs). Effect of PVN-BL was assessed before, right after i.p. injection of OTR antagonist L-368,899 (1 mg/kg) and after its washout (n=6). Effect of CNO (3 mg/kg) was measured 1 h after i.p. injection and its 24 h washout (n=10).

Statistical significance: ***** p<0.05, ****** p<0.01, one-way ANOVA followed by Tukey's multiple comparison post-hoc test.

Figure 7. The role of the novel type of parvOT neurons in coordinating central and peripheral OT release to promote analgesia.

We hypothesize that pain stimulates the identified subset of parvOT PVN neurons, which simultaneously release OT in the SON and SC, exerting

respectively delayed and longer lasting and immediate and shorter lasting analgesia. The peripheral analgesic effect of OT is likely mediated by its action on blood brain barrier-free sensory neurons of the dorsal root ganglion (DRG).

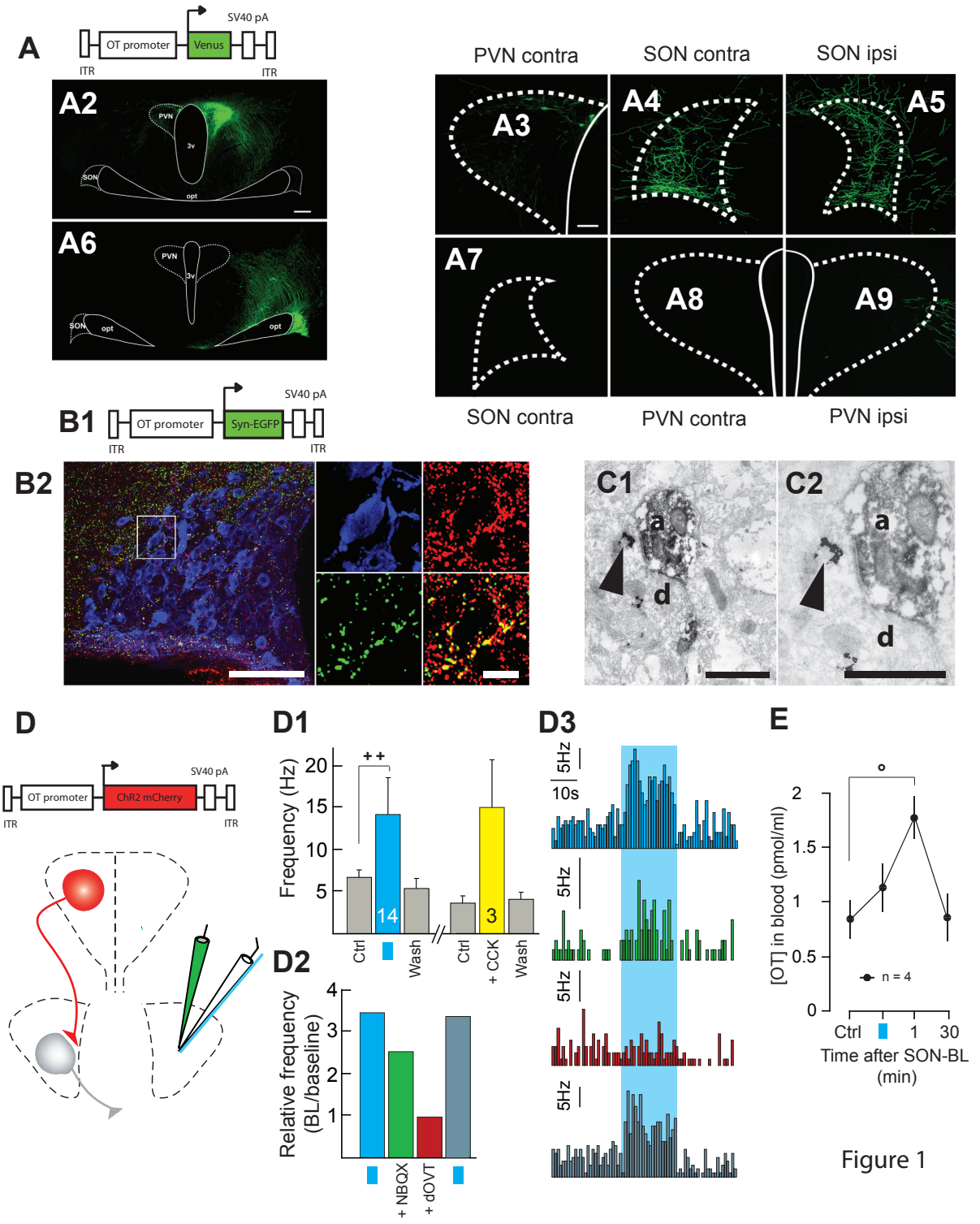
A
SV40 pA
OT promoter
Venus
ITR
ITR
A2
PVN
3v
SON
opt
A6
PVN
3v
SON
opt
opt
PVN contra
SON contra
SON ipsi
A3
A4
A5
A7
A8
A9
SON contra
PVN contra
PVN ipsi
B1
SV40 pA
OT promoter
Syn-EGFP
ITR
ITR
B2
C1
a
d
C2
a
d
D
SV40 pA
OT promoter
ChR2 mCherry
ITR
ITR
D1
Frequency (Hz)
20
15
10
5
++
14
3
Ctrl
Wash
Ctrl
+ CCK
Wash
D2
Relative frequency (BL/baseline)
4
3
2
1
+ NBQX
+ dOVT
D3
5Hz
10s
5Hz
5Hz
5Hz
E
[OT] in blood (pmol/ml)
2
1.5
1
0.5
0
n = 4
Ctrl
1
30
Time after SON-BL (min)

Figure 1

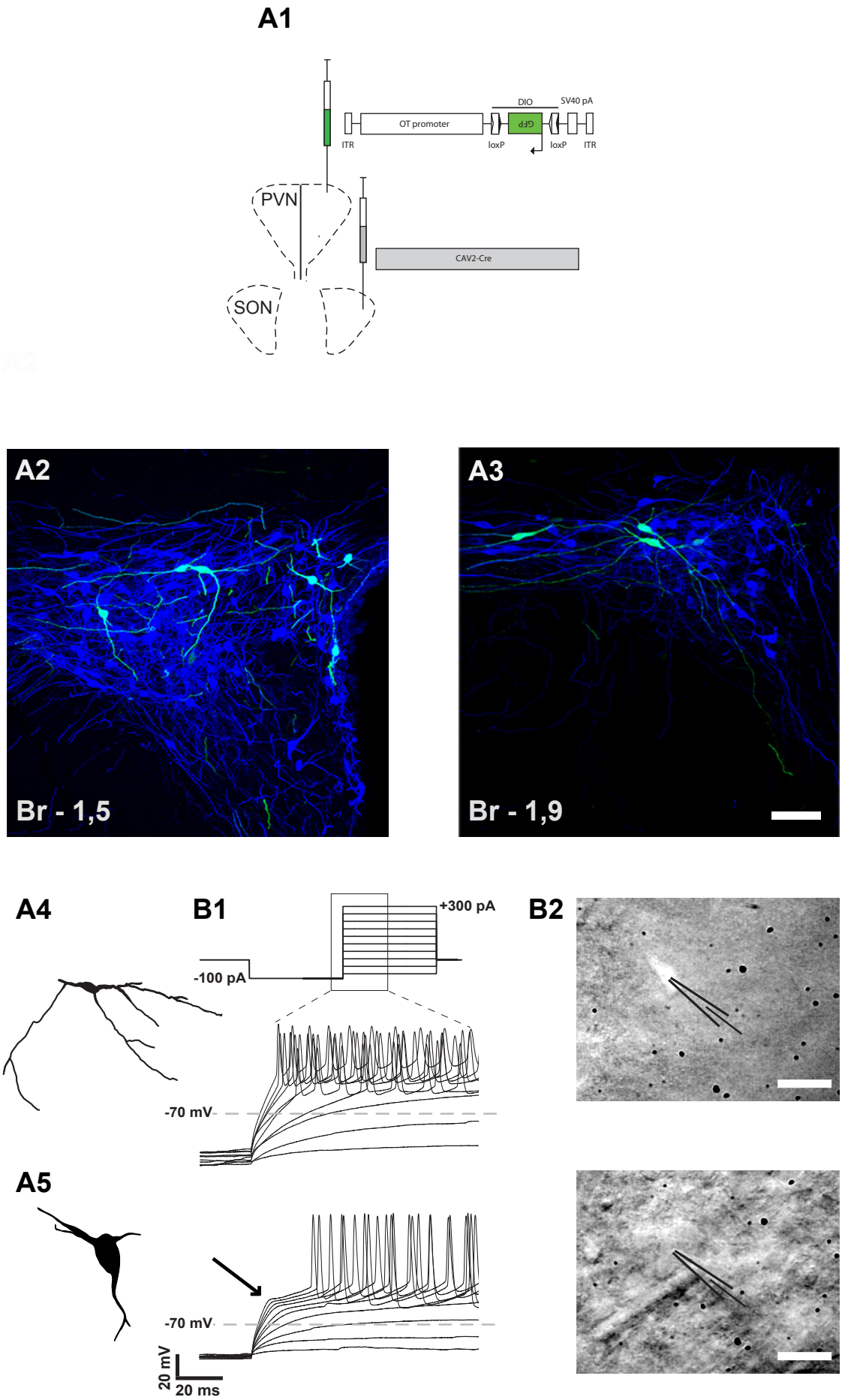
A1
DIO
SV40 pA
OT promoter
GFP
ITR
loxP
loxP
ITR
PVN
CAV2-Cre
SON
A2
Br - 1,5
A3
Br - 1,9
A4
B1
+300 pA
-100 pA
-70 mV
B2
A5
-70 mV
20 mV
20 ms

Figure 2

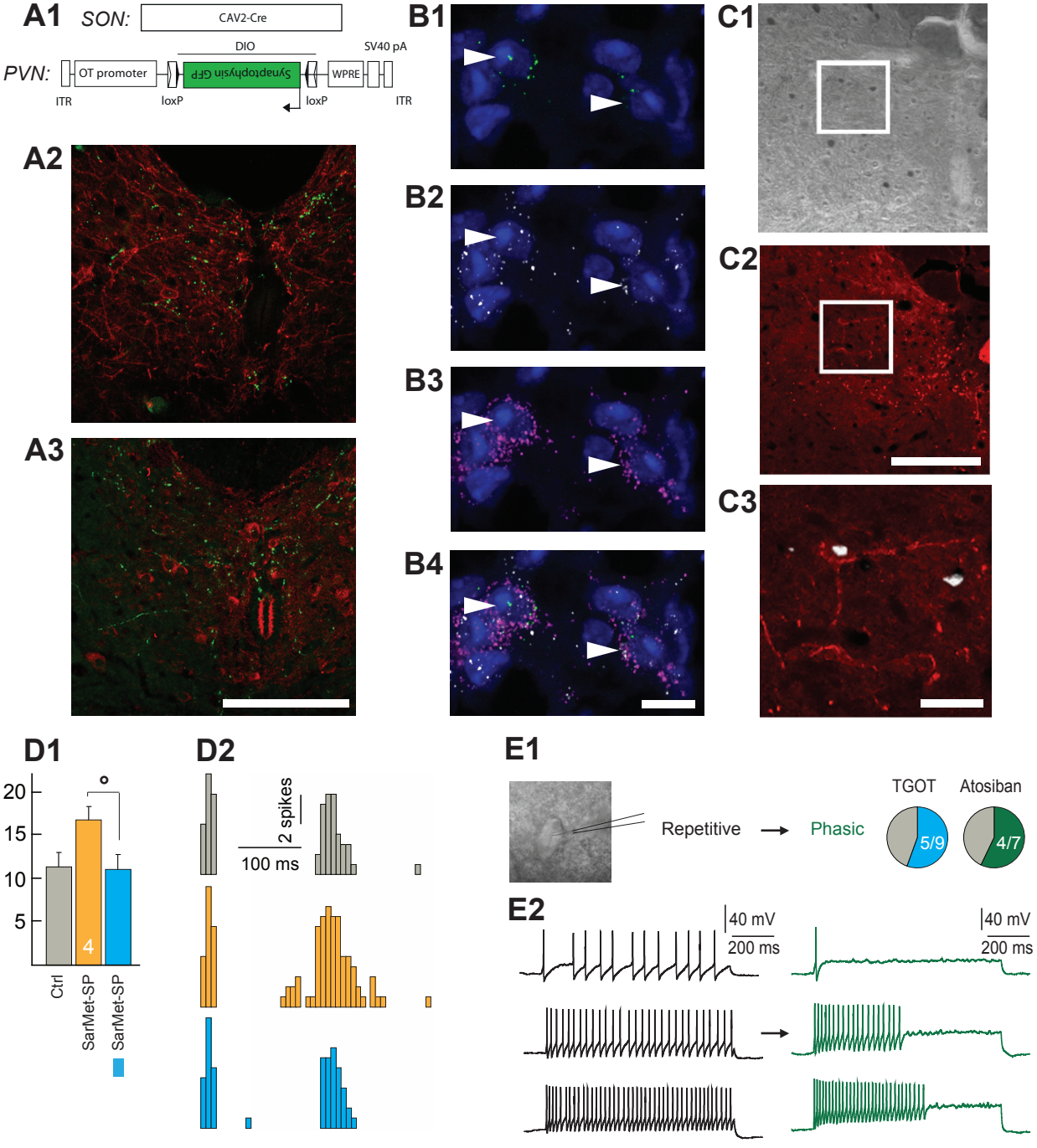
A1
SON:
CAV2-Cre
DIO
SV40 pA
PVN:
OT promoter
Synaptophysin GFP
WPRE
ITR
loxP
loxP
ITR
A2
A3
B1
B2
B3
B4
C1
C2
C3
D1
D2
Spikes / stim
20
15
10
5
4
Ctrl
SarMet-SP
SarMet-SP
2 spikes
100 ms
E1
Repetitive
Phasic
TGOT
Atosiban
5/9
4/7
E2
40 mV
200 ms
40 mV
200 ms

Figure 3

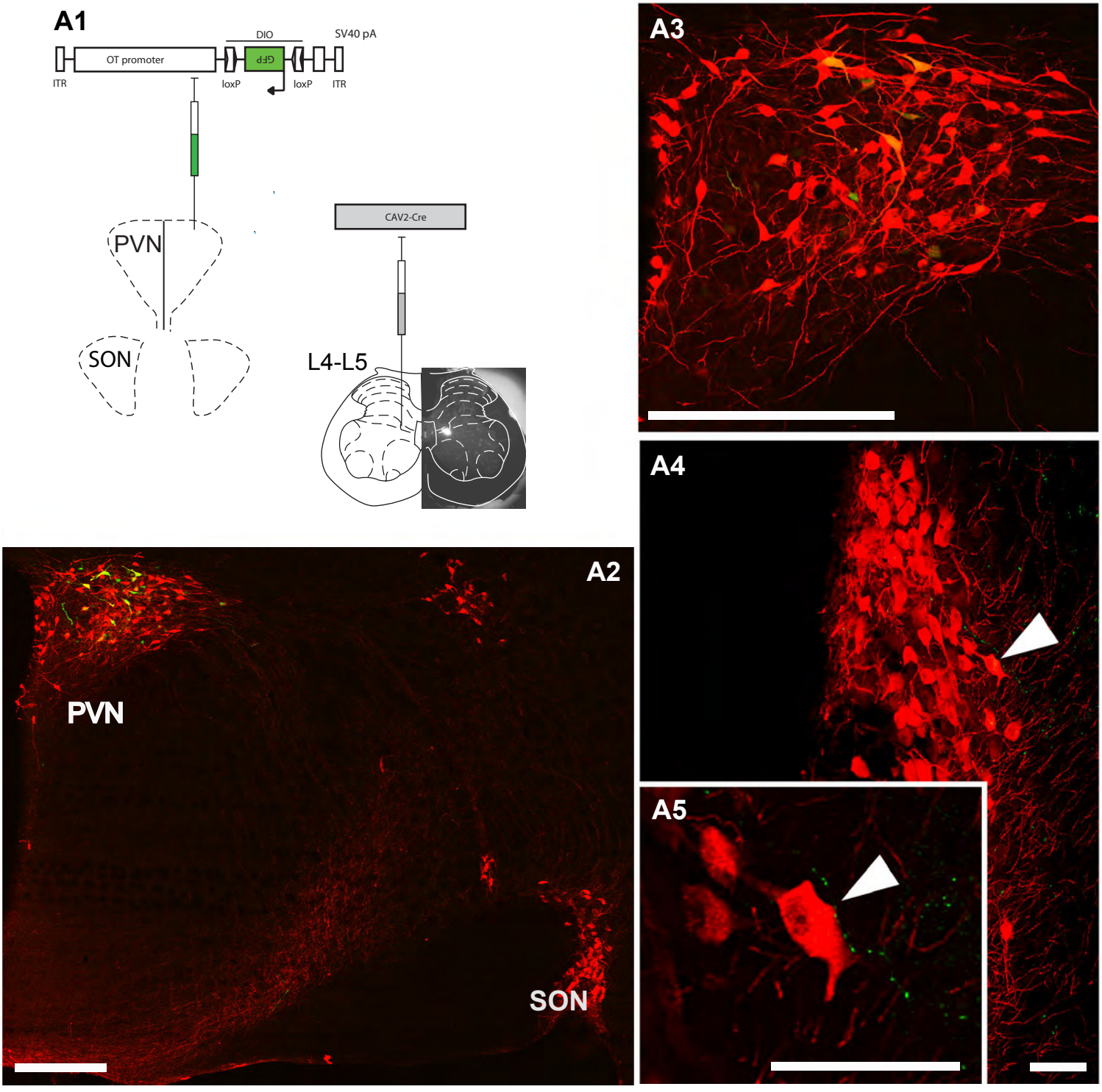
A1
DIO
SV40 pA
OT promoter
GFP
ITR
loxP
loxP
ITR
PVN
SON
CAV2-Cre
L4-L5
A3
A4
A5
A2
PVN
SON

Figure 4

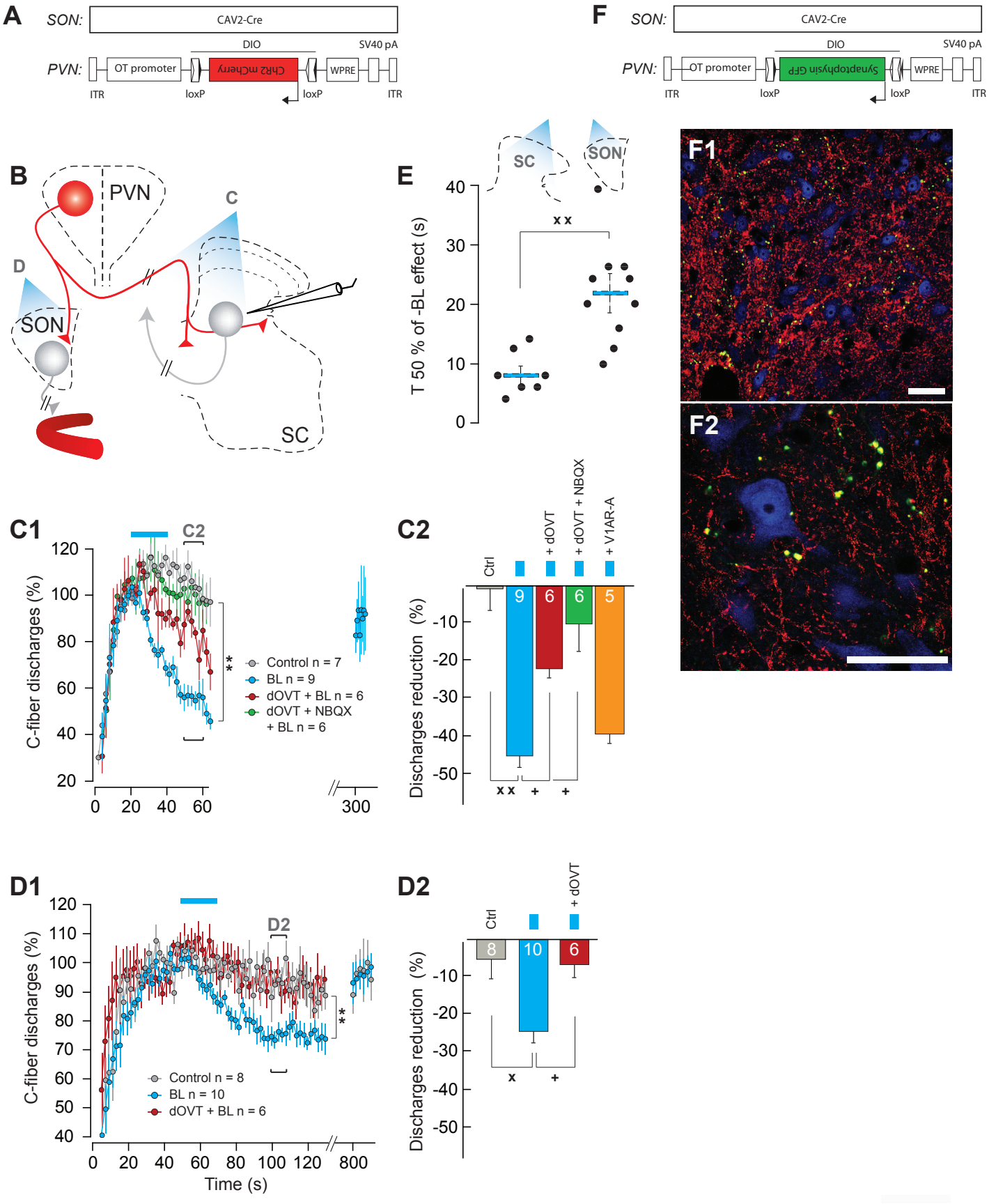
A
SON:
CAV2-Cre
DIO
SV40 pA
PVN:
OT promoter
ChR2 mCherry
WPRE
ITR
loxP
loxP
ITR
F
SON:
CAV2-Cre
DIO
SV40 pA
PVN:
OT promoter
Synaptophysin GFP
WPRE
ITR
loxP
loxP
ITR
B
PVN
C
D
SON
SC
E
SC
SON
T 50 % of -BL effect (s)
40
30
20
10
0
x x
F1
F2
C1
C2
C-fiber discharges (%)
120
100
80
60
40
20
0
20
40
60
300
**
Control n = 7
BL n = 9
dOVT + BL n = 6
dOVT + NBQX
+ BL n = 6
C2
Ctrl
+ dOVT
+ dOVT + NBQX
+ V1AR-A
Discharges reduction (%)
-10
-20
-30
-40
-50
9
6
6
5
x x
+
+
D1
D2
C-fiber discharges (%)
120
110
100
90
80
70
60
50
40
0
20
40
60
80
100
120
800
Time (s)
**
Control n = 8
BL n = 10
dOVT + BL n = 6
D2
Ctrl
+ dOVT
Discharges reduction (%)
-10
-20
-30
-40
-50
8
10
6
x
+

Figure 5

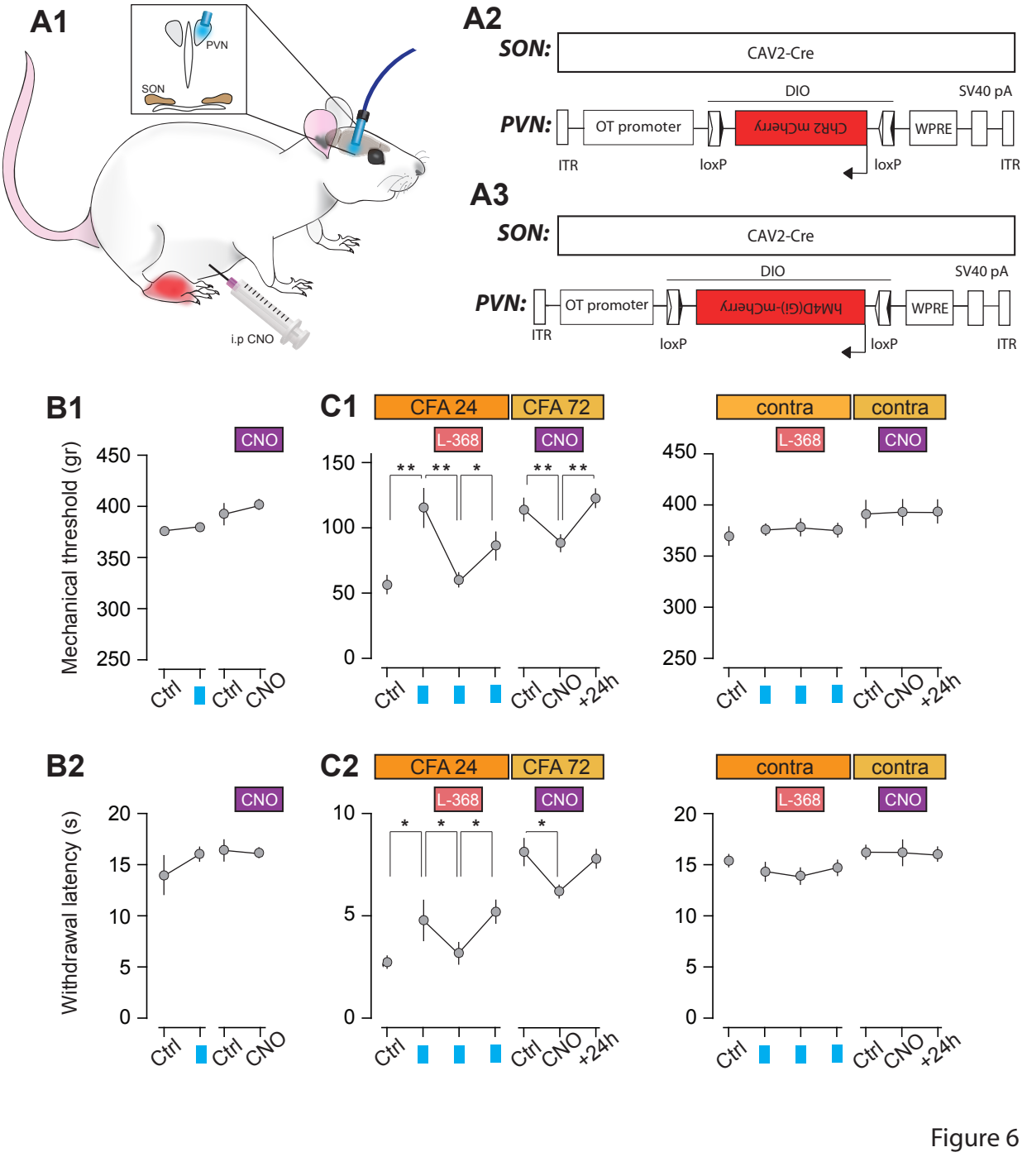
A1
PVN
SON
i.p CNO
A2
SON:
CAV2-Cre
DIO
SV40 pA
PVN:
OT promoter
ChR2 mCherry
WPRE
ITR
loxP
loxP
ITR
A3
SON:
CAV2-Cre
DIO
SV40 pA
PVN:
OT promoter
hM4D(Gi)-mCherry
WPRE
ITR
loxP
loxP
ITR
B1
Mechanical threshold (gr)
CNO
Ctrl
Ctrl
CNO
C1
CFA 24
CFA 72
L-368
CNO
contra
contra
Ctrl
CNO
+24h
B2
Withdrawal latency (s)
C2

Figure 6

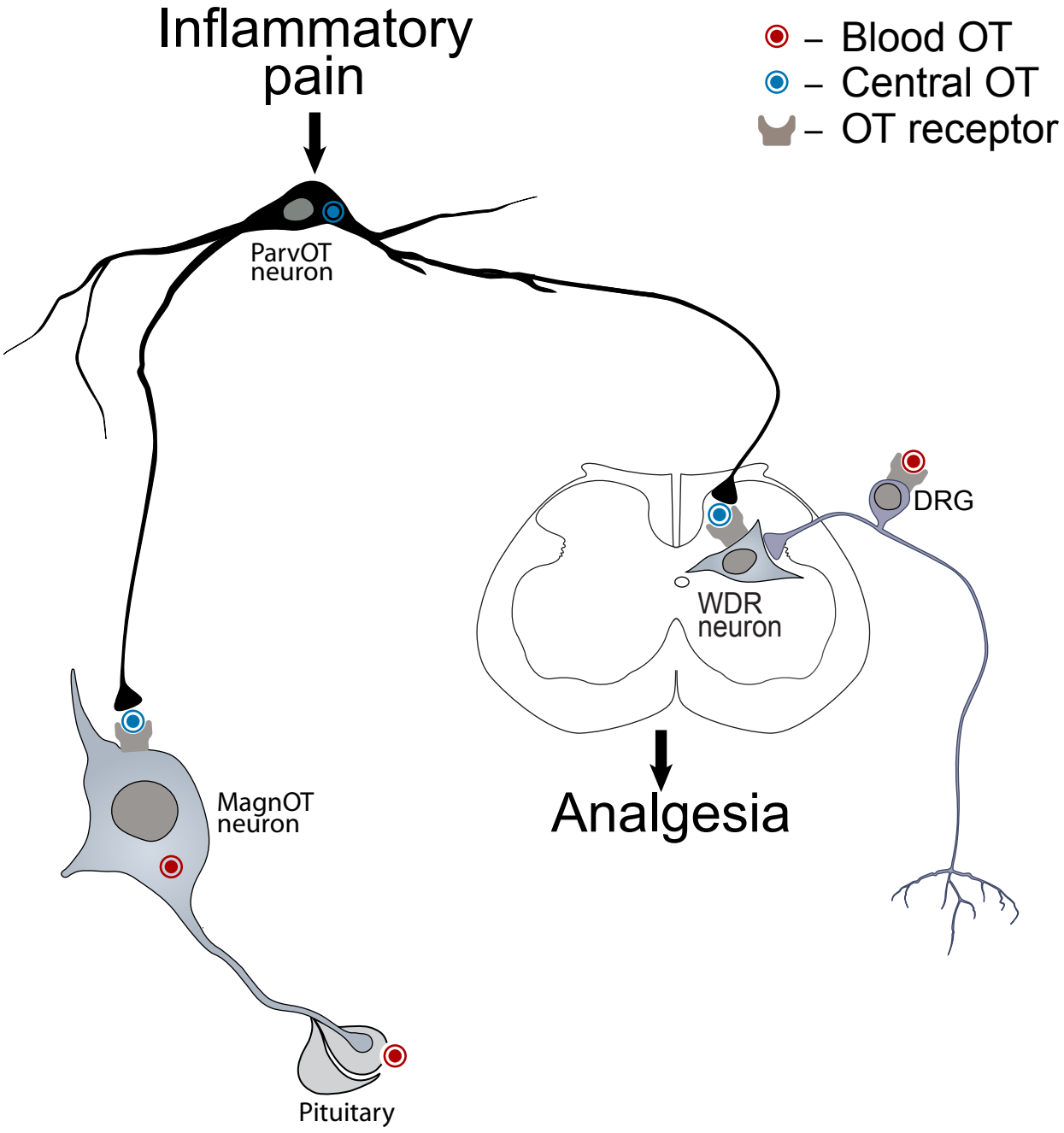
Inflammatory pain
– Blood OT
– Central OT
– OT receptor
ParvOT neuron
DRG
WDR neuron
MagnOT neuron
Analgesia
Pituitary

Figure 7